

# Propulsion of a chiral swimmer in viscoelastic fluids

Takuya Kobayashi, John J. Molina, and Ryoichi Yamamoto\*

Department of Chemical Engineering, Kyoto University, Kyoto 615-8510, Japan

(Dated: November 13, 2023)

Microswimmers often use chirality to generate translational movement from rotational motion. We study the swimming velocity of a spherical chiral microswimmer and find that the self-propulsion velocity increases quadratically with the degree of chirality in viscoelastic fluids. We show that this speed enhancement is caused by the normal stress differences that are generated by the rotational flows around the microswimmer, which lead to a Weissenberg effect. Furthermore, the normal stress difference is swimmer-specific, i.e., it will depend on whether the swimmer is a pusher or a puller.

Naturally occurring microswimmers, such as bacteria [1] and sperm cells [2–4], often swim through complex biological fluids characterized by non-Newtonian behavior. These non-Newtonian environments differ fundamentally from purely viscous Newtonian fluids. One well-known example is the rheological phenomenon known as the Weissenberg effect [5], whereby viscoelastic fluids will climb up a rotating rod due to the normal stress differences. Furthermore, it is well-established that microswimmers behave differently in complex fluids compared to Newtonian fluids [3, 6–10]. Previous experimental, theoretical and simulation studies have demonstrated the impact of elasticity on the swimming speeds of various microswimmers in complex viscoelastic fluids [11–26]. Understanding the underlying mechanisms of these phenomena, in particular, and the role of hydrodynamic interactions, in general, is necessary to explain and control the complex behavior of microswimmers in viscoelastic fluids. This knowledge holds significant relevance across multiple domains, including applications in biomedicine, e.g. for targeted drug delivery [27, 28].

Previous experiments have revealed that the presence of polymer in a solution can alter the behavior of *E. coli* cells [6], which exhibit counterclockwise flagellar rotation and clockwise body rotation during swimming [29], resulting in a chiral flow. In particular, they found that the cells tumble less and their velocity increases in a polymer solution. In this letter, to understand such behavior, we focus on elucidating the enhanced swimming speed of chiral microswimmers, a phenomenon first reported by Binagia *et al.* [24] and later confirmed by Housiadas *et al.* [25] through theory and simulations. Remarkably, recent experimental, theoretical and simulation work demonstrated that micro-robots can swim in viscoelastic fluids by applying this same principle [30]. In their study, a micro-robot, consisting of counter-rotating head and tail spheres, failed to swim in a Newtonian fluid but could do so in a viscoelastic fluid. These results emphasize how the first normal stress difference in viscoelastic fluids plays a crucial role in boosting the swimming speeds [24, 25, 30]. However, the precise mechanisms underlying the generation of the normal stress differences by the swimmer’s chirality and their impact on swimming speed remain unclear.

Furthermore, previous theoretical and simulation studies [18, 21, 22, 26], using the squirmer model, have shown that the swimming speed varies with the swimmer type (pusher, puller or neutral) in viscoelastic fluids. In contrast, in Newtonian fluids at low Reynolds numbers, the swimming speed is relatively insensitive to the swimmer’s type [31]. In addition, the swimming speed is known to be smaller in a Giesekus fluid than in a Newtonian fluid, for all swimmer types, primarily due to the presence of the non-Newtonian elongational stress [18]. The mechanisms responsible for this swimmer-type dependence of the swimming speed in various viscoelastic fluids remains to be determined.

In this Letter, to understand the influence of the fluid elasticity on the swimming speed, we conducted direct numerical simulations of a squirmer in an Oldroyd-B fluid. Here, we demonstrate that the Weissenberg effect, arising from the first normal stress difference (NSD) generated by the swimmer’s chirality, is responsible for the swimming speed enhancement. Additionally, we investigated the variation in swimming speed based on the swimmer type and found that the first NSD is also responsible for the swimmer-type dependence of the swimming speed.

In the squirmer model [32, 33], the propulsion is generated by imposing a modified slip velocity at the particle’s surface. Specifically, we consider the first two polar modes  $B_1$  and  $B_2$ , along with the second azimuthal mode  $C_2$ , the so-called rotlet dipole. This consideration leads to the following expression for the slip velocity [34] (Fig. 1):

$$\begin{aligned} \mathbf{u}^{\text{sq}}(\theta, \varphi) &= \left( B_1 \sin \theta + \frac{B_2}{2} \sin 2\theta \right) \hat{\boldsymbol{\theta}} + \frac{3}{2} C_2 \sin 2\theta \hat{\boldsymbol{\varphi}} \\ &= B_1 \left[ \left( \sin \theta + \frac{\alpha}{2} \sin 2\theta \right) \hat{\boldsymbol{\theta}} + \frac{3}{2} \zeta \sin 2\theta \hat{\boldsymbol{\varphi}} \right] \end{aligned} \quad (1)$$

with  $\theta$  and  $\varphi$  the polar and azimuthal angles,  $\hat{\boldsymbol{\theta}}$  and  $\hat{\boldsymbol{\varphi}}$  the corresponding unit tangent vectors. The first polar mode  $B_1$  determines the steady swimming speed in a Newtonian fluid, expressed as  $U_N = 2/3B_1$ . Furthermore, the ratios  $\alpha = B_2/B_1$  and  $\zeta = C_2/B_1$  represent the swimmer type and the strength of the flow chirality, respectively.

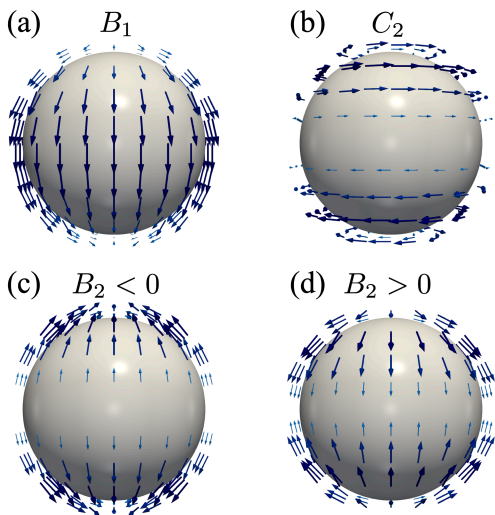


FIG. 1. Schematic representation of the surface slip velocity of each mode, (a) $B_1$ , (c, d) $B_2$  and (b) $C_2$ .

Swimmers with  $\alpha < 0$  are called pushers (e.g., *E.coli.*), which generate an extensile flow field in the swimming direction. On the other hand,  $\alpha > 0$  denotes pullers (e.g., *Chlamydomonas*), which generate a contractile flow field. Squirmers with  $\alpha = 0$  are termed neutral swimmers, and swim with a potential flow field. The chiral parameter  $\zeta$  generates the flow pattern of a microswimmer with rotating flagella and a counter-rotating body [24, 25, 35].

We employed the Smoothed Profile (SP) method [36, 37] to fully resolve the fluid-particle hydrodynamic coupling. This method has been employed to investigate the dynamics of colloids and microswimmers in viscoelastic fluids [26, 38, 39]. In this method, the sharp boundary between the particle and fluid is replaced with a continuous diffuse interface of thickness  $\xi$ , by introducing a smoothed profile function  $\phi \in [0, 1]$ , which is 1 inside the particle and 0 outside. The mathematical definition of  $\phi$  can be found in Ref. [36]. Introducing this  $\phi$  field allows us to define field variables for all particle quantities. The fluid-particle coupling is then accounted for by enforcing the momentum conservation between fluid and particle domains. In particular, the total velocity  $\mathbf{u} = \mathbf{u}_f + \mathbf{u}_p$ , including the host fluid  $\mathbf{u}_f$  and particle contributions  $\mathbf{u}_p$ , is governed by a modified Navier-Stokes equation

$$\rho \left( \frac{\partial}{\partial t} + \mathbf{u} \cdot \nabla \right) \mathbf{u} = -\nabla p + \nabla \cdot \boldsymbol{\sigma} + \rho(\phi \mathbf{f}_p + \phi \mathbf{f}_{sq}) \quad (3)$$

with the incompressible condition  $\nabla \cdot \mathbf{u} = 0$ , where  $\rho$  is the fluid mass density,  $p$  is the pressure,  $\boldsymbol{\sigma}$  is the stress tensor,  $\phi \mathbf{f}_p$  is a body force applied to enforce the particle's rigidity, and  $\phi \mathbf{f}_{sq}$  is the force due to the squirming motion. For the viscoelastic fluid, we adopt the Oldroyd-B model ( $\boldsymbol{\sigma} = \boldsymbol{\sigma}_s + \boldsymbol{\sigma}_p$ ), which is a generalization of

the Newtonian fluid,  $\boldsymbol{\sigma}_s = \eta_s [\nabla \mathbf{u} + (\nabla \mathbf{u})^T]$ , and the Upper Convected Maxwell (UCM) fluid,  $\boldsymbol{\sigma}_p + \lambda \overset{\nabla}{\boldsymbol{\sigma}}_p = \eta_p [\nabla \mathbf{u} + (\nabla \mathbf{u})^T]$ , where  $\eta_s$  and  $\eta_p$  are the viscosities of the Newtonian solvent and the viscoelastic solute, respectively,  $\lambda$  is the polymer relaxation time, and  $\overset{\nabla}{\boldsymbol{\sigma}}$  is the upper-convected derivative, given by  $\overset{\nabla}{\boldsymbol{\sigma}} = \partial_t \boldsymbol{\sigma} + \mathbf{u} \cdot \nabla \boldsymbol{\sigma} - (\nabla \mathbf{u})^T \cdot \boldsymbol{\sigma} - \boldsymbol{\sigma} \cdot (\nabla \mathbf{u})$ .

The (spherical) particles follow the Newton-Euler equations of motion, given by

$$\dot{\mathbf{R}}_i = \mathbf{V}_i, \quad \dot{\mathbf{Q}}_i = \text{skew}(\boldsymbol{\Omega}_i) \cdot \mathbf{Q}_i \quad (4)$$

$$M_i \dot{\mathbf{V}}_i = \mathbf{F}_i^H + \mathbf{F}_i^{sq}, \quad \mathbf{I}_p \cdot \dot{\boldsymbol{\Omega}}_i = \mathbf{N}_i^H + \mathbf{N}_i^{sq} \quad (5)$$

where  $\mathbf{R}_i$  and  $\mathbf{V}_i$  are the position and velocity of particle  $i$ , respectively, and  $\mathbf{Q}_i$  and  $\boldsymbol{\Omega}_i$  the orientation matrix and angular velocity. The hydrodynamic forces and torques are denoted as  $\mathbf{F}_i^H$  and  $\mathbf{N}_i^H$ , respectively, while  $\mathbf{F}_i^{sq}$  and  $\mathbf{N}_i^{sq}$  represent the force and torque due to the squirming motion. The function  $\text{skew}(\boldsymbol{\Omega}_i)$  is used to create the skew-symmetric matrix of the angular velocity  $\boldsymbol{\Omega}_i$ , which is defined as:

$$\text{skew}(\boldsymbol{\Omega}) = \begin{pmatrix} 0 & -\Omega_z & \Omega_y \\ \Omega_z & 0 & -\Omega_x \\ -\Omega_y & \Omega_x & 0 \end{pmatrix} \quad (6)$$

Further details can be found in Ref. [26].

We performed simulations for a single neutral squirmer, radius  $a = 4\Delta$  and interface width  $\xi = 2\Delta$ , inside a cubic simulation box of length  $L = 64\Delta$  ( $\Delta$  represents the grid spacing), with periodic boundary conditions in all directions. These simulations were performed for different chiral parameters  $\zeta$ , in both Newtonian and Oldroyd-B fluids. The host fluids have a mass density and zero-shear viscosity of  $\rho = \eta_0 = 1$ . The particle Reynolds number, Weissenberg number and the viscosity ratio are  $\text{Re} = \rho U_N a / \eta_0 = 0.01$ ,  $\text{Wi} = \lambda B_1 / a = 0.2$  and  $\beta = \eta_s / \eta_0 = \eta_s / (\eta_s + \eta_p) = 0.5$ , respectively. It is observed that the swimming velocity in viscoelastic fluids exhibits a quadratic dependence on the chiral parameter  $\zeta$  (see Fig. 2(a)). This speed-up is in consistent with that reported for Gisekus fluid [24] and Oldroyd-B fluids [25]. In contrast, the velocity remains constant in Newtonian fluids, regardless of  $\zeta$ , since the  $C_2$  term is decoupled from the translational motion for a spherical particle. To quantify this relationship between the swimming speed and the swimmer's chirality, we fit our simulation results to the following simple function of  $\zeta$ ,  $\beta$  and  $\text{Wi}$ :

$$\frac{U(\zeta)}{U(0)} = 1 + \beta(1 - \beta)\text{Wi}^2 \zeta^2 \quad (7)$$

We have compared our results with the expressions derived by Housiadas *et al.* [25], but we note that their results were obtained for an unbounded system at  $\text{Re} = 0$ ,

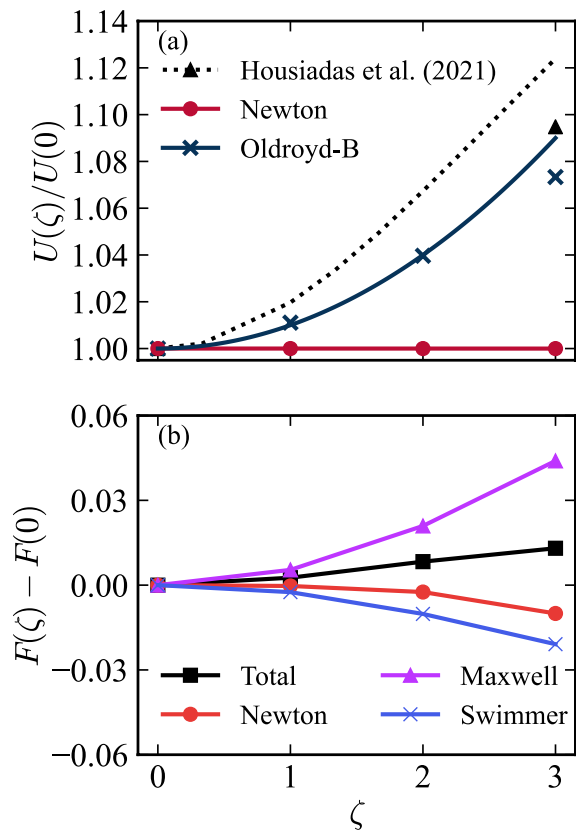


FIG. 2. (a) Nondimensional swimming speed of an isolated neutral squirmer as a function of the chiral parameter  $\zeta$  in a Newtonian fluid (red) and an Oldroyd-B fluid (blue). The symbols are simulation results and the solid lines represent Eq. (7). The dotted line and triangle symbol are the analytical solution and numerical results obtained by Housiadas *et al.* [25] in an Oldroyd-B fluid, respectively. (b) Force difference from the force at  $\zeta = 0$  on a fixed squirmer in an Oldroyd-B fluid, as a function of the chiral parameter  $\zeta$  with the force being parallel to the swimming axis.

whereas we have used a small, but non-zero,  $\text{Re} = 0.01$ , with periodic boundary conditions.

In order to unveil the mechanism behind this swimming speed enhancement, we shift our focus to the force contributions parallel to the swimming axis on a fixed squirmer. As shown in Fig. 2(b), the total force increases with the chiral parameter  $\zeta$ , similar to the swimming speed. Furthermore, the force contributions arising from the Newtonian stress  $\sigma_s$  and squirming motion both decrease with the chiral parameter  $\zeta$ . In contrast, the contribution due to the Maxwell stress  $\sigma_p$  increases with the chiral parameter  $\zeta$ . Therefore, we can conclude that the Maxwell contribution is the primary mechanism responsible for the swimming speed enhancement.

To clarify how the Maxwell stress contributes to the total force, we considered the role of the normal stress differences (NSD), which have been previously reported to enhance the swimming speed [24, 25, 30]. It is worth

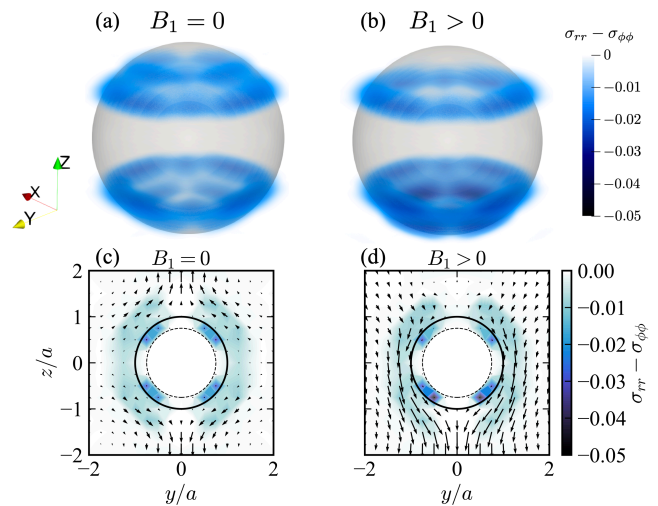


FIG. 3. Velocity and first normal stress difference (NSD)  $\sigma_{rr} - \sigma_{\phi\phi}$  fields around a squirmer particle. (a) and (c) correspond to a squirmer with  $B_1 = 0$ , while (b) and (d) correspond to  $B_1 > 0$ . In (c) and (d), the quiver plot shows the velocity field, and the density map represents the NSD field. The dashed lines represent the position of  $r = a - \xi/2$ .

noting that the main distinction between Newtonian and Oldroyd-B fluids lies in the presence of the first NSD. The force per unit area on a squirmer, in spherical coordinates, is given by the first NSD

$$(\sigma_f \cdot \mathbf{n})_r = \sigma_{rr} - p = \sigma_{rr} - \sigma_{\phi\phi} + \text{const.} \quad (8)$$

By considering only the rotlet dipole ( $C_2$  term) in Eq. (1) and taking into account rotational symmetry in the  $\phi$  direction,  $\partial_\phi(-p + \sigma_{\phi\phi}) = 0$ .

As shown in Fig. 3, this first NSD  $\sigma_{rr} - \sigma_{\phi\phi}$ , generated by the squirmer's chirality, adopts a ring-shaped distribution near the north/south poles. In turn, this results in a net force directed towards the center of the squirmer. When  $B_1 = 0$ , the NSD field is symmetric between the upper and lower hemispheres. Thus, the NSD works towards reducing/enhancing the swimming speed in the upper/lower hemispheres, however, given the symmetry, these two contributions balance each other and result in a net zero total force.

However, when  $B_1 \neq 0$ , the asymmetry of the velocity field between the upper and lower hemispheres, generated by the asymmetry of the  $B_1$  term (as described in Eq. (1)), leads to a top-bottom asymmetry in the normal stress differences. In particular, the absolute value of the NSD on the lower hemisphere is greater than that on the upper hemisphere. The NSD thus works towards reducing/enhancing the swimming speed in the upper/lower hemispheres, with the force on the lower hemisphere being greater, which leads to the swimming speed enhancement in viscoelastic fluids.

In Fig. 3, we plot the velocity and first NSD fields around the particle, which illustrate the Weissenberg ef-

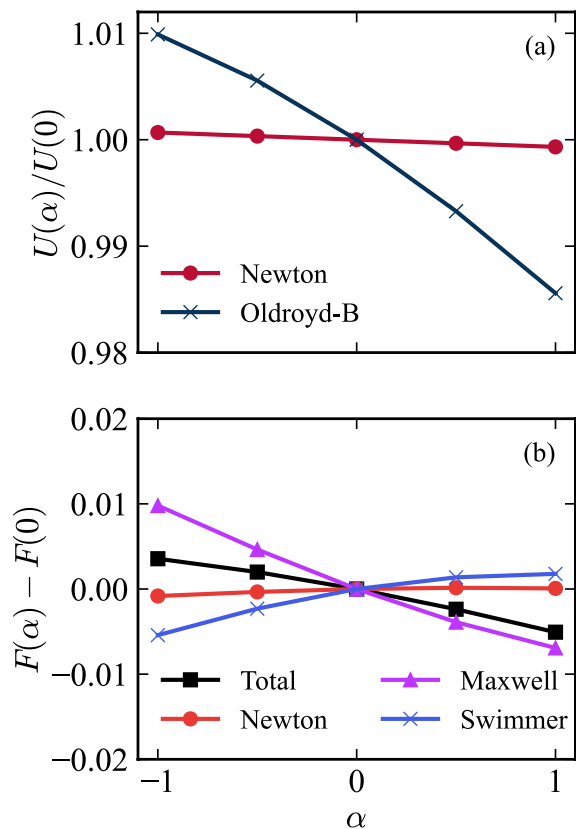


FIG. 4. (a) Nondimensional swimming speed of an isolated squirmer as a function of the swimming type  $\alpha$  in both a Newtonian fluid (red) and an Oldroyd-B fluid (blue). (b) Force difference from the force at  $\alpha = 0$  on a fixed squirmer in an Oldroyd-B fluid as a function of the swimmer type  $\alpha$ , with the force being parallel to the swimming axis.

fect arising from the counter-rotating flows in the upper/lower hemispheres. This results in the particle pushing the fluid upward and downward symmetrically along the swimming axis, when  $B_1 = 0$ . However, when  $B_1 > 0$ , this Weissenberg effect occurs asymmetrically, due to the asymmetry of the first NSD, which will tend to accelerate the squirmer in an Oldroyd-B fluid.

Next, we conducted simulations for a single non-chiral squirmer ( $\zeta = 0$ ), with  $a = 8\Delta$  and  $\xi = 2\Delta$  within a fully periodic cubic simulation box of length  $L = 64\Delta$ . The particle Reynolds number, Weissenberg number, and viscosity ratio are  $Re = 0.01$ ,  $Wi = 0.1$ , and  $\beta = 0.5$ , respectively.

The swimming speeds for a squirmer as a function of the swimmer type  $\alpha$  are shown in Fig. 4(a). In a Newtonian fluid, the swimming speed is independent of the swimming type, with a weak  $Re$  dependence, which can be approximated by  $U/U_N \simeq 1 - 0.15\alpha Re$  [31]. This is consistent with our observed results. In contrast, in an Oldroyd-B fluid, the swimming speed of a squirmer decreases with  $\alpha$ , with pushers ( $\alpha < 0$ ) swimming faster

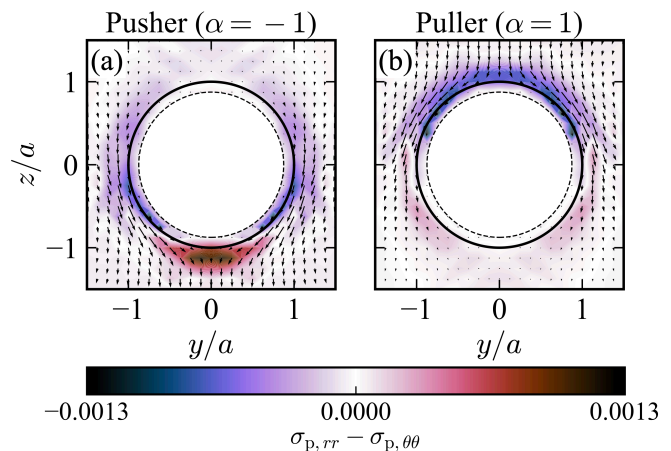


FIG. 5. Velocity field and first normal stress difference  $\sigma_{rr} - \sigma_{\theta\theta}$  for (a) a pusher with  $\alpha = -1$  and (b) a puller with  $\alpha = 1$ . The quiver plot shows the velocity field and the density map represents the NSD field. The dashed lines represent the position of  $r = a - \xi/2$ .

than pullers ( $\alpha > 0$ ). This observation closely resembles the perturbation expansion in terms of  $Wi$  for the UCM fluid (an Oldroyd-B fluid with  $\eta_s = 0$ ), which is expressed as  $U/U_N = 1 - 0.2\alpha Wi$  [22]. Remarkably, this trend holds despite the difference in the fluids (i.e., constitutive relations).

We again analyzed the force contributions parallel to the swimming axis on a fixed squirmer. As shown in Fig. 4(b), the force decreases with  $\alpha$ , as does the swimming speed. We find that pushers swim faster than pullers due to the decrease in the Maxwell contribution with the  $\alpha$  parameter. To clarify this decrease in the Maxwell contribution to the force with  $\alpha$ , we investigated the NSD around a pusher with  $\alpha = -1$  and a puller with  $\alpha = 1$ . As illustrated in Fig. 5, for a pusher, the NSD due to uniaxial elongation at  $\theta = \pi$  works towards reducing the swimming speed, while the NSD due to the shear flow at  $\theta \simeq 3\pi/4$  can enhance the swimming speed. On the other hand, for a puller, both the NSD due to biaxial elongation at  $\theta = 0$  and the NSD due to the shear flow at  $\theta \simeq \pi/4$  work towards reducing the swimming speed. Therefore, the swimming speed dependence on the swimming type  $\alpha$  is associated with the direction of the force generated by the shear flow in an Oldroyd-B fluid, while it is related to the force generated by the elongational flow in a Giesekus fluid [18].

In this letter, we have investigated the impact of fluid elasticity on swimming speed, uncovering non-trivial velocity variations that are not observed in Newtonian fluids but are present in Oldroyd-B fluids. We observed that the swimming velocity increases quadratically with the chiral parameter  $\zeta$  in viscoelastic fluids, see Eq. (7). The primary mechanism responsible for the speed-up due to the squirmer's chirality is the first NSD, lead-

ing to the Weissenberg effect. Previously, we found that, due to the squirmer's chirality, this swimming speed enhancement occurs for all swimmer types (pusher, puller or neutral) [26]. When considering variations in swimming speed based on swimmer type, the first NSD generates forces that accelerate pushers and decelerate pullers. This explains why pushers swim faster than pullers in Oldroyd-B fluids.

The authors would like to thank Prof. Takashi Taniguchi for fruitful discussions. This work was supported by the Grants-in-Aid for Scientific Research (JSPS KAKENHI) under grant nos. JP 20H00129, 20H05619, 20K03786, and by JST SPRING, grant no. JPMJSP2110.

---

\* ryoichi@cheme.kyoto-u.ac.jp

- [1] S. M. Sillankorva, H. Oliveira, and J. Azeredo, *Int. J. Microbiol.* **2012**, 863945 (2012).
- [2] D. F. Katz, R. N. Mills, and T. R. Pritchett, *J. Reprod. Fertil.* **53**, 259 (1978).
- [3] L. J. Fauci and R. Dillon, *Annu. Rev. Fluid Mech.* **38**, 371 (2006).
- [4] S. S. Suarez and A. A. Pacey, *Hum. Reprod. Update* **12**, 23 (2006).
- [5] K. Weissenberg, *Nature* **159**, 310 (1947).
- [6] A. E. Patteson, A. Gopinath, M. Goulian, and P. E. Arratia, *Sci. Rep.* **5**, 15761 (2015).
- [7] A. E. Patteson, A. Gopinath, and P. E. Arratia, *Curr. Opin. Colloid Interface Sci.* **21**, 86 (2016).
- [8] C.-K. Tung, C. Lin, B. Harvey, A. G. Fiore, F. Ardon, M. Wu, and S. S. Suarez, *Sci. Rep.* **7**, 3152 (2017).
- [9] G. Li, E. Lauga, and A. M. Ardekani, *J. Non-Newtonian Fluid Mech.* **297**, 104655 (2021).
- [10] S. Kamdar, S. Shin, P. Leishangthem, L. F. Francis, X. Xu, and X. Cheng, *Nature* **603**, 819 (2022).
- [11] H. C. Fu, T. R. Powers, and C. W. Wolgemuth, *Phys. Rev. Lett.* **99**, 258101 (2007).
- [12] E. Lauga, *Phys. Fluids* **19**, 083104 (2007).
- [13] H. C. Fu, C. W. Wolgemuth, and T. R. Powers, *Phys. Fluids* **21**, 33102 (2009).
- [14] J. Teran, L. Fauci, and M. Shelley, *Phys. Rev. Lett.* **104**, 038101 (2010).
- [15] X. N. Shen and P. E. Arratia, *Phys. Rev. Lett.* **106**, 208101 (2011).
- [16] B. Liu, T. R. Powers, and K. S. Breuer, *Proc. Natl. Acad. Sci. U. S. A.* **108**, 19516 (2011).
- [17] L. Zhu, M. Do-Quang, E. Lauga, and L. Brandt, *Phys. Rev. E* **83**, 011901 (2011).
- [18] L. Zhu, E. Lauga, and L. Brandt, *Phys. Fluids* **24**, 051902 (2012).
- [19] S. E. Spagnolie, B. Liu, and T. R. Powers, *Phys. Rev. Lett.* **111**, 068101 (2013).
- [20] E. E. Riley and E. Lauga, *EPL* **108**, 34003 (2014).
- [21] M. De Corato, F. Greco, and P. L. Maffettone, *Phys. Rev. E Stat. Nonlin. Soft Matter Phys.* **92**, 053008 (2015).
- [22] C. Datt and G. J. Elfring, *J. Non-Newtonian Fluid Mech.* **270**, 51 (2019).
- [23] J. P. Binagia, C. J. Guido, and E. S. G. Shaqfeh, *Soft Matter* **15**, 4836 (2019).
- [24] J. P. Binagia, A. Phoa, K. D. Housiadas, and E. S. G. Shaqfeh, *J. Fluid Mech.* **900** (2020).
- [25] K. D. Housiadas, J. P. Binagia, and E. S. G. Shaqfeh, *J. Fluid Mech.* **911** (2021).
- [26] T. Kobayashi, G. Jung, Y. Matsuoka, Y. Nakayama, J. J. Molina, and R. Yamamoto, *Soft Matter* **19**, 7109 (2023).
- [27] D. Patra, S. Sengupta, W. Duan, H. Zhang, R. Pavlick, and A. Sen, *Nanoscale* **5**, 1273 (2013).
- [28] W. Gao and J. Wang, *Nanoscale* **6**, 10486 (2014).
- [29] E. Lauga, *Annu. Rev. Fluid Mech.* **48**, 105 (2016).
- [30] L. A. Kroo, J. P. Binagia, N. Eckman, M. Prakash, and E. S. G. Shaqfeh, *J. Fluid Mech.* **944**, A20 (2022).
- [31] S. Wang and A. Ardekani, *Phys. Fluids* **24**, 101902 (2012).
- [32] M. J. Lighthill, *Commun. Pure Appl. Math.* **5**, 109 (1952).
- [33] J. R. Blake, *J. Fluid Mech.* **46**, 199 (1971).
- [34] O. S. Pak and E. Lauga, *J. Eng. Math.* **88**, 1 (2014).
- [35] F. Fadda, J. J. Molina, and R. Yamamoto, *Phys. Rev. E* **101**, 052608 (2020).
- [36] Y. Nakayama and R. Yamamoto, *Phys. Rev. E* **71**, 036707 (2005).
- [37] R. Yamamoto, J. J. Molina, and Y. Nakayama, *Soft Matter* **17**, 4226 (2021).
- [38] Y. Matsuoka, Y. Nakayama, and T. Kajiwara, *Soft Matter* **16**, 728 (2020).
- [39] Y. Matsuoka, Y. Nakayama, and T. Kajiwara, *Journal of Fluid Mechanics* **913**, A38 (2021).